Journal of Chromatography A, 1218 (2011) 1942–1953

Contents lists available at ScienceDirect

Journal of Chromatography A

journal homepage: www.elsevier.com/locate/chroma

Structural variation of solid core and thickness of porous shell of 1.7 μm core–shell silica particles on chromatographic performance: Narrow bore columns

Jesse O. Omamogho [a], John P. Hanrahan [b], Joe Tobin [b], Jeremy D. Glennon [a,*]

[a] Innovative Chromatography Group, Irish Separation Science Cluster (ISSC), Department of Chemistry and the Analytical, Biological and Chemistry Research Facility (ABCRF), University College Cork, Cork, Ireland
[b] Glantreo Ltd., ERI Building, Lee Road, Cork, Ireland

ARTICLE INFO

Article history:
Available online 4 December 2010

Keywords:
EIROSHELL™
Core–shell
Shell thickness
1.7 μm
Extra-column variance

ABSTRACT

Chromatographic and mass transfer kinetic properties of three narrow bore columns (2.1 × 50 mm) packed with new core–shell 1.7 μm EIROSHELL™-C_{18} (EiS-C_{18}) particles have been studied. The particles in each column varied in the solid-core to shell particle size ratio (ρ), of 0.59, 0.71 and 0.82, with a porous silica shell thickness of 350, 250 and 150 nm respectively. Scanning and transmission electron microscopy (SEM and TEM), Coulter counter analysis, gas pycnometry, nitrogen sorption analysis and inverse size exclusion chromatography (ISEC) elucidated the physical properties of these materials. The porosity measurement of the packed HILIC and C_{18} modified phases provided the means to estimate the phase ratios of the three different shell columns (EiS-150-C_{18}, EiS-250-C_{18} and EiS-350-C_{18}). The dependence of the chromatographic performance to the volume fraction of the porous shell was observed for all three columns. The naphtho[2,3-a]pyrene retention factor of $k' \sim 10$ on the three EiS-C_{18s} employed to obtain the height equivalents to theoretical plates (HETPs) data were achieved by varying the mobile phase compositions and applying the Wilke and Chang relationship to obtain a parallel reduced linear velocity. The Knox fit model gave the coefficient of the reduce HETPs for the three EiS-C_{18s}. The reduced plate height minimum $h_{min} = 1.9$ was achieved for the EiS-150-C_{18} column, and generated an efficiency of over 350,000 N/m and $h_{min} = 2.5$ equivalent to an efficiency of 200,000 N/m for the EiS-350-C_{18} column. The efficiency loss of the EiS-C18 column emanating from the system extra-column volume was discussed with respect to the porous shell thickness.

1. Introduction

In the recent development of particle technology targeted for liquid chromatography, the use of shell particles has received considerable attention. The development of core–shell particles is pivotal to modern liquid chromatography (LC) column technology. The launch of the Fused-Core® particles (Halo™) in 2006 by Advanced Material Technology (AMT) marked the beginning of a new dawn in chromatography column [1]. The Halo is a 2.7 μm silica particle, consisting of 1.7 μm non-porous particles and 0.5 μm porous shell The Halo column generates an efficiency of 250,000 N/m equivalent to reduce plate height minimum (h_{min}) of 1.5 for small molecules when packed in a 4.6 mm I.D. columns [2]. The overall particle size larger than 2 μm provides the Halo column with an advantage over the sub-2 μm particles to operate satisfactorily on conventional LC systems because of their larger inherent permeability [3]. This advantage also allows column coupling leading to significant gain in efficiency, particularly for the separations of complex mixtures [4]. In 2009, Phenomenex® has begun to offer silica core–shell particles of 2.6 and 1.7 μm particle diameters. The 2.6 μm consists of a 1.9 μm nonporous particles coated with a 0.35 μm porous layer of aggregated colloidal silica. Similarly, the 1.7 μm consists of a 1.3 μm solid-core covered with a 0.25 μm porous layers of silica. These columns are currently commercialized as Kinetex™ [5]. The 2.6 μm is capable of producing an efficiency of 320,000 N/m, equivalent to $h_{min} = 1.2$ when packed in a 4.6 mm I.D. column [6,7]. It produces up to 200,000 N/m, equivalent to $h_{min} \sim 1.9$ when packed in a narrow bore column, i.e., a 2.1 mm I.D. column [5].

The Kinetex 1.7 μm particle column produces an efficiency of 280,000 N/m, equivalent to $h_{min} = 2.0$ when packed in a 2.1 mm I.D. column [8], comparable to the sub-2 μm totally porous particles. The porous layer thickness plays a significant role in the overall separation mechanism. For example, two 3.0 μm particle

* Corresponding author. Tel.: +353 214902669.
E-mail address: j.glennon@ucc.ie (J.D. Glennon).

0021-9673/$ – see front matter © 2010 Elsevier B.V. All rights reserved.
doi:10.1016/j.chroma.2010.11.067

diameter with different porous shell thicknesses with a similar reversed phase liquid chromatography (RPLC) surface coverage and pore size will exhibit different rates of mass transfer phenomenon and phase equilibrium thermodynamics. The thinner the porous shell the faster the separation analysis time, resulting in improved efficiency [9] The detailed factors contributing to the improved efficiency of columns packed with shell particles are quite complex, such that the conventional kinetic (van Deemter's and Knox's equation) method of analysis based on fit model rarely give the precise kinetic information [10]. It is best to simplify that the zone spreading in RPLC columns is significantly minimized when the porous shell thickness is thinner. The disadvantage of columns packed with thin porous shell particles is the strong sensitivity to extra-column volume contribution attenuating the efficiency significantly, particularly when packed in narrow bore columns. The extra-column variance contribution from the instrument must be taken into account and subtracted from the overall variance derived from the system and columns. The extra-column variance can be over 50% (depending on the instrument configuration) of the total variance, resulting in a significant loss of efficiency [11].

The first modern theoretical model described by Kaczmarski and Guiochon [12] takes into account the influence of thickness of porous layers of shell particles on the chromatographic performance. The authors emphasised on the mass transfer resistance (C-term) of large molecules such as protein. Fundamental studies of the physical properties of shell particles are paramount to correlate the intrinsic separation performance of columns packed with these new materials. The benchmark of the separation performance is provided by columns packed with shell particles [7]. To establish the cause of this groundbreaking performance, a series of independent and complimentary analyses, ranging from physicochemical and mass transfer kinetic properties was employed to compare for two commercially available shell columns [13]. The kinetic performance of columns packed with shell particles is governed by the systematic variation of the properties of the porous layers, and most importantly by the porous layer thickness surrounding the solid core segment of the shell particles.

Recently a comparative study of the kinetic performance of narrow bore columns of sub-2 μm shell particle based on the 1.7 μm Kinetex-C_{18} and the fully porous particle of 1.7 μm BEH-C_{18} (Waters, MA) reveals some concern regarding the influence of narrow bore I.D. columns on the overall efficiency [8]. Notice that the reduced height equivalent to a theoretical plate (HETP) for the narrow bore columns was $h_{min} \sim 2.0$ [8]. Two recent reports studying and comparing the kinetic performance of shell particles as a function of variation of the shell thickness provide some important information about the beneficial role of the shell thickness of the core–shell particles based on columns supplied from different manufacturers [7,13]. Such a study lacks some minor but crucial element necessary to provide a linear correlation of particle intrinsic morphology to their independent physical properties. To illustrate this point, the Halo 2.7 μm particle has a shell thickness of 0.5 μm, corresponding to 80% volume fraction of the porous layer whereas the Kinetex 2.6 μm has a porous shell thickness of 0.35 μm, equivalent to 58% of the porous volume fraction of the particle. This makes the Halo 2.7 μm 28% larger on porous volume fraction than the Kinetex 2.6 μm. However, the total porosity measured on these two materials does not reflect the correlation to the intrinsic values of their porous volume fraction. The difference in the total porosity of the HILIC column was 8% higher for the Halo 2.7 μm than the Kinetex 2.6 μm column [13]. Hence this uncorrelated physical property of the columns of Kinetex and Halo particle is expected to result in a similar or smaller B-term for the latter. In addition, the surface roughness also varies significantly among the Halo and Kinetex particles, accounting for wide differences in the overall C-term due to a large local variation of the external film mass transfer resistance. A large variation on the A-term is also observed due to local differences on the surface roughness among columns packed with the Halo and Kinetex particles. The rougher surface of the Halo particles improves column packing homogeneity due to less slippage between particles during bed consolidation [13].

In an attempt to make a direct comparison of the influence of the thickness of porous layers and to eliminate the uncorrelated variations of the intrinsic physicochemical properties of shell particles that may arise due to different manufacturing processes, we have prepared core–shell particles based on a unique approach, referred to as seeded growth mesoporous shell (SGMS) layering [14]. The core–shell particle is branded EIROSHELL™ (Glantreo Ltd., Ireland). The aim is to provide a tailored control of surface morphology of the shell particles during the stages of synthesis to maintain a linear correlation of the physical properties. Ultimately, conclusions on the chromatographic kinetic performance can be attributed wholly to the variation of the porous layer thickness of the core–shell particles. For the first time, three 1.7 μm core–shell particles that vary linearly in the porous shell thickness and the solid core are studied: (a) 1.0 μm solid core, 0.35 μm shell thickness, (b) 1.2 μm solid core, 0.25 μm shell thickness, and (c) 1.4 μm solid core, 0.15 μm shell thickness. The external surfaces of these three materials are equally smooth with a pore sizes of ~90 Å.

2. Experimental

2.1. Characterisation

The external surface morphology was measured using the high resolution Inspect™ F50 (FEI Company Europe) scanning electron microscope (SEM) at 20 kV; detailed imaging analysis of the internal solid core and the shell layer morphology was performed using the JEM-2000FX (Jeol, UK Ltd.) transmission electron microscope (TEM) at 200 kV. The surface area, pore size and pore size distribution and pore volume measurements of the three EIROSHELL™ 1.7 μm particles were performed based on the gas sorption technique using the Micromeritics Gemini V.2380 surface area analyzer (Micromeritics, Norcross, GA, USA). The surface area was analysed based on the Brunauer–Emmett–Teller (BET) method [15]; the pore volume, pore size and pore size distribution were measured based on the Barrett–Joyner–Halenda (BJH) method [16]. The pore volume was measured at a single point for $P/P_o > 0.39$. An average of five measurements of the three EIROSHELL™ 1.7 μm particle size distribution based on Electric Sensing Zone (ESZ) method was performed using the Multisizer™ 3 Coulter counter enhanced by the Digital Pulse Processor (DPP). The measurement of the skeletal density of the EiS-C_{18} particles was taken from five average runs using the AccuPyc 1340 gas pycnometer (Micromeritics, Norcross, GA, USA). Elemental and thermogravimetric analyses to determine the percentage of carbon present on the naked and modified C_{18} EiS silica were performed using the CE440 elemental analyser (Exeter Analytical (UK) Ltd.) and the TGA/DSC-1 Thermogravimetric analyzer (Mettler Toledo AG, Switzerland) respectively. Column packing was carried out by Glantreo Ltd. (Cork, Ireland). Chromatographic data were recorded using the Agilent 1200 RRLC system; data points for the HETPs for each column were fitted using the Knox equation.

2.2. Reagents and chemicals

All chemicals and reagents were used as supplied from the manufacturers. Octadecyldimethylchlorosilane (97%), imidazole (99%), HPLC grade methanol (99.9%), naphtho[2,3-a]pyrene (98%) were purchased from Sigma–Aldrich (Dublin, Ireland). Uracil (99%),

acetophenone (99.5%), benzene (99.9%), toluene (99.8% anhydrous) and naphthalene (+99% scintillation grade) were purchased from Sigma–Aldrich (Dublin, Ireland). Polystyrene standard kits (GPC) (MW = 475; 1920; 3250; 10,250; 24,000; 32,500; 67,500; 160,000; 295,000; 705,000; 1,000,000; and 2,180,000) were also purchased from Sigma–Aldrich (Dublin, Ireland). Deionized water was obtained from a Milli-Q water purification system (Millipore) with resistivity of 18.2 MΩ cm.

2.3. Synthesis of C_{18} bonded phases and column packing

The synthesis of 1.7 μm EIROSHELL™ silica particles with a controlled thickness of the porous layers based on a proprietary method is described elsewhere [14]. The C_{18} bonded phases were prepared on the three 1.7 μm EIROSHELL™ silica particle using mono functional octadecyldimethylchlorosilane ligand ($C_{20}H_{43}Si_1Cl_1$) under controlled reflux condition as reported in Ref. [17], using toluene as the reaction solvent and the reflux reaction time was 6 h. The resulting C_{18} bonded stationary phases were denoted as EiS-350-C_{18}, EiS-250-C_{18} and EiS-150-C_{18}, Narrow bore columns (2.1 I.D. × 50 mm) were packed separately with both naked and C_{18} bonded EiS particles using the low viscosity slurry packing technique [18]. In brief, 0.22 g of stationary phase silica was slurried in 20 mL of 50/50 (v/v%) methanol/chloroform and transferred to a 20 mL slurry packing reservoir. The slurry was packed using methanol at a flow rate of 25–5 mL/min. Most importantly during the packing, a relatively constant pressure is maintained. Prior to column packing, the weight of the empty columns including the frits and end-fittings was measured on a balance displaying the mass rounded to 4 decimal places. After the packing was completed, the columns were closed tightly with the frits and end-fittings inserted. The unplugged columns were dried in a desiccator containing phosphorus pentoxide (P_2O_5) as the desiccant for 24 h under vacuum created by a water aspirator by the Venturi effect. The weight differences measured for each column after vacuum drying for 24 h were between approximately 50–43%. To ensure that all the packing solvents had been completely evacuated from the columns, they were subjected to a further 24 h of vacuum drying. No loss of weight was observed, indicating that the initial 24 h was sufficient to evacuate all packing solvents present in the packed columns. The ease of this practice is the fact that the packing solvent is quite volatile (methanol), thus promoting the complete evacuation at a relatively shorter time under vacuum desiccation. Knowing the weight of the columns, the mass of the stationary phase packing material was determined (see Table 3).

2.4. Column evaluations and measurement of HETP data

Chromatography studies were carried out to evaluate the separation performance of the EiS-350-C_{18}, EiS-250-C_{18} and EiS-150-C_{18} phases packed in 2.1 I.D. × 50 mm columns. The chromatography of a mixture of non-polar small molecules was evaluated on the three shell columns under identical mobile phase composition and conditions (50/50, v/v% acetonitrile/water, 25 °C and at flow rate of 0.4 mL/min). The following test solutes were used: (1) uracil (90 μg/mL), (2) acetophenone (150 μg/mL), (3) benzene (1500 μg/mL), (4) toluene (6500 μg/mL), (5) naphthalene (500 μg/mL). A injection volume of 0.3 μL was used and the detection was UV = 254 nm with a sampling rate of 80 Hz and a peak response time of 20 ms.

0.3 μL of a dilute sample of naphtho[2,3-a]pyrene in pure acetonitrile was used to obtain the HETP data for the study of the kinetic performance of the three 1.7 μm EiS-C_{18} columns. The HETP for each column was measured at the same retention factor by varying the mobile phase composition used for the flow studies. The mobile phase composition was 85/15 (v/v%) acetonitrile/water for the EiS-350-C_{18} column; 78/22 (v/v%) acetonitrile/water for the EiS-250-C_{18} column and 70/30 (v/v%) acetonitrile/water for the EiS-150-C_{18} column. The Wilke and Chang equation [19] is used to estimate the molecular diffusivity of the naphtho[2,3-a]pyrene extended to the mixtures of eluent for the three different mobile phase compositions used to study the HETPs for each EiS-C_{18} columns

$$D_m = 7.4 \times 10^{-8} \frac{\sqrt{x_{ACN}\psi_{ACN}M_{ACN} + x_{HO}\psi_{H_2O}M_{H_2O}}}{\eta V_A^{0.6}} T \quad (1)$$

V_A is the molar volume of naphtho[2,3-a]pyrene at its boiling point (V_A = 152.4 cm^3/mol), was estimated based on the Schroeder and Le Bas method as updated by Sastri et al. [20], M_{ACN} = 41 g/mol and M_{H_2O} = 18 g/mol, are the molecular weights of acetonitrile and water, ψ_{ACN} = 1 and ψ_{H_2O} = 2.6 are the solvent association factor for acetonitrile and water, x_{ACN} and x_{H_2O} are the molar fraction of acetonitrile and water in the mobile phase respectively, η is the viscosity of the mobile phase (η = 0.50, 0.56 and 0.64) for mixture of acetonitrile/water (85/15, 78/22, and 70/30 (v/v%) at 295 K, respectively), and T is the temperature in Kelvin. The peak profiles were acquired at frequencies of 10–80 Hz and response rates of 100–20 ms using the Agilent 1200 RRLC UV detection at 298 nm.

The system extra-column volume from the injector to the column entry and from the column exit to the detector flow cell is 10.5 μL (when the column is replaced with a zero dead volume connector). The HETPs were measured using the peak apex as the retention time and the peak width at half height, assuming the peak shapes of the analytes are Gaussian under the experimental conditions selected. It was corrected for the extra-column volume by injecting naptho[2,3-a]pyrene (at the same concentration and injection volume for the measurement of HETP data) through a zero dead volume connector at each flow rates and mobile phase conditions the HETP study. The fitted HETP data are given according to the following equation [7]:

$$H = L\frac{\left(t^r_{1/2} - t^f_{1/2}\right)^2 - \left(t^r_{1/2,e} - t^f_{1/2,e}\right)^2}{5.545(t_R - t_e)^2} \quad (2)$$

where $t^r_{1/2}$, $t^f_{1/2}$ are the rear and front width of the measured peak at half height respectively with the column connected, $t^r_{1/2,e}$, $t^f_{1/2,e}$ are the rear and front width of the measured peak at half height respectively without the column, t_R and t_e are the retention time recorded for the peak apices of the test compound (acenaphthene) with and without column respectively.

The extra-column volume peak variance ($\mu'_{2,ex}$) given as μL^2 was measured using the half peak width as follows:

$$\mu'_{2,ex} = F_v^2 \frac{\left(t^r_{1/2} - t^f_{1/2}\right)^2}{5.545} \quad (3)$$

where F_v is flow rate (μL/min). The variance of the Agilent 1200 RRLC (after optimization) was between 3.5 and 4.0 μL^2, depending on the mobile phase composition. The small values of extra-column variance measured from this instrument are due to the modification made. For example, we changed the capillary tubing from 0.17 mm I.D. to 0.11 mm I.D. and the flow cell was changed from 6 μL to 1.7 μL. This affords a reduced system extra-column volume.

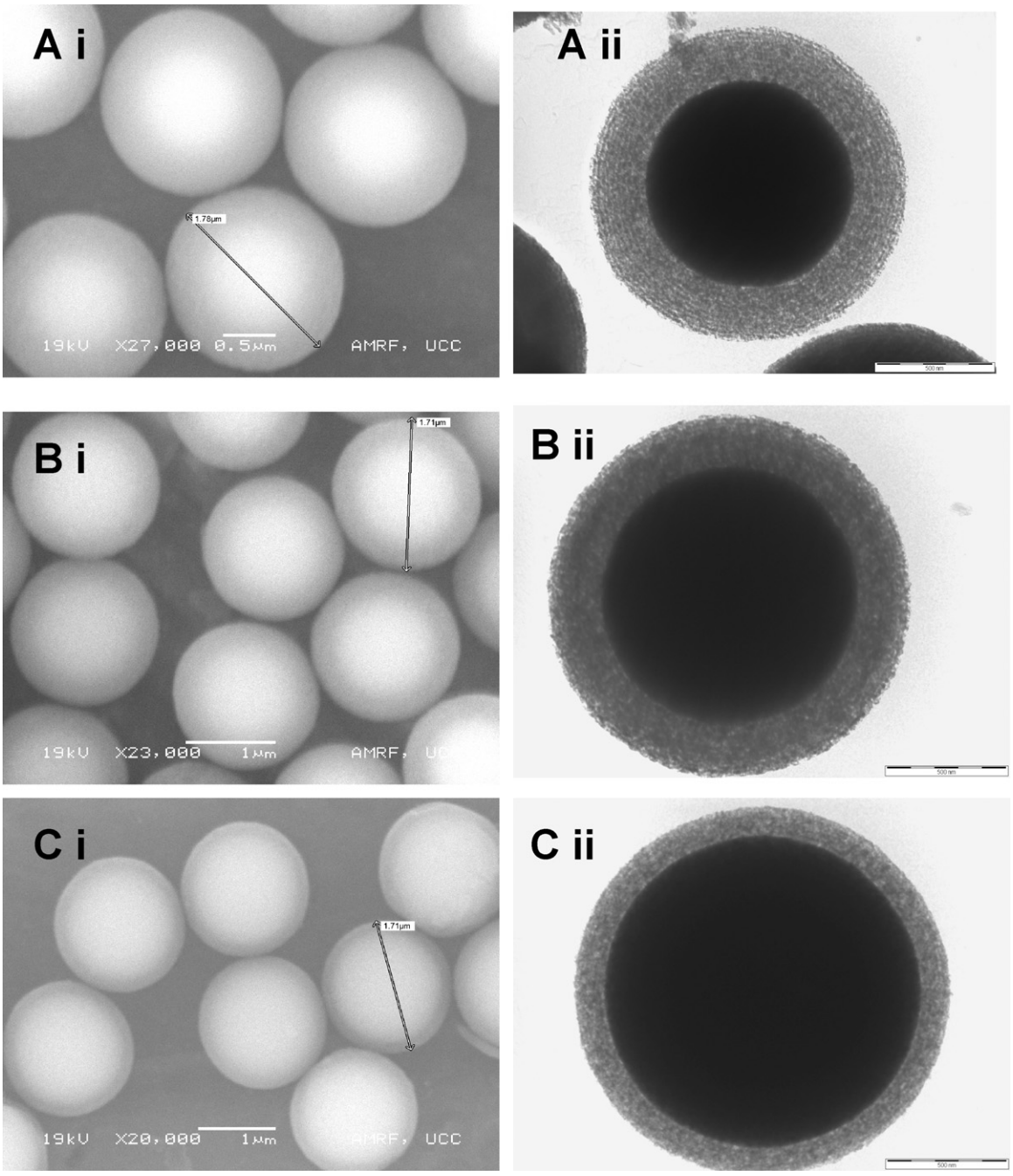

Fig. 1. Electron micrograph of three EIROSHELL^{TM} 1.7 μm particles (Ai) SEM of EiS-350 and (Aii) TEM of EiS-350; (Bi) SEM of EiS-250 and (Bii) TEM of EiS-250; (Ci) SEM of EiS-150 and (Cii) TEM of EiS-150. Note the stratified structure that is clearly visible on the EiS-350 shell particle indicating uniform layering of the silica shells.

3. Results and discussion

3.1. Physical characterisation of the EiS-350, 250 and 150 core–shell particles

3.1.1. Electron microscopy imaging

The three EIROSHELL^{TM} 1.7 μm (EiS-1.7 μm) core–shell silica particles synthesised are highly spherical in shape as revealed by scanning electron microscopy (SEM) as shown in Fig. 1. The porous layer thickness of the three EIROSHELL^{TM} particles varies by changing the diameter of the solid-core to have a common core–shell particle diameter of 1.7 μm. The porous shell layers of the three EiS-1.7 μm are 0.35 μm, 0.25 μm and 0.15 μm with solid core diameter of 1.0 μm, 1.2 μm and 1.4 μm respectively. The three EIROSHELL^{TM} particles studied are identified as EiS-350, EiS-250 and EiS-150. Transmission electron microscopy (TEM) micrographs of the individual EiS-350 to EiS-150 particles are shown in Fig. 1Aii–Cii. The images reveal a contrast between the solid core and the porous layers of the EiS particles. The TEM was also able to provide some physical characteristics of the porous shell layers such as multi-layering patterning of porous shell silica perpendicular to the solid core substructure. The TEM ability to reveal the well-defined contrasting features between the solid core and the porous shell layer could be due to the penetrating power of the high tension (HT) beam at 200 keV. The intrinsic morphology of the porous and non-porous structure of the EiS particles resulted in random scattering of the TEM electron beam. The scattering in the solid-core is predominantly inelastic causing the primary electron beam to interact

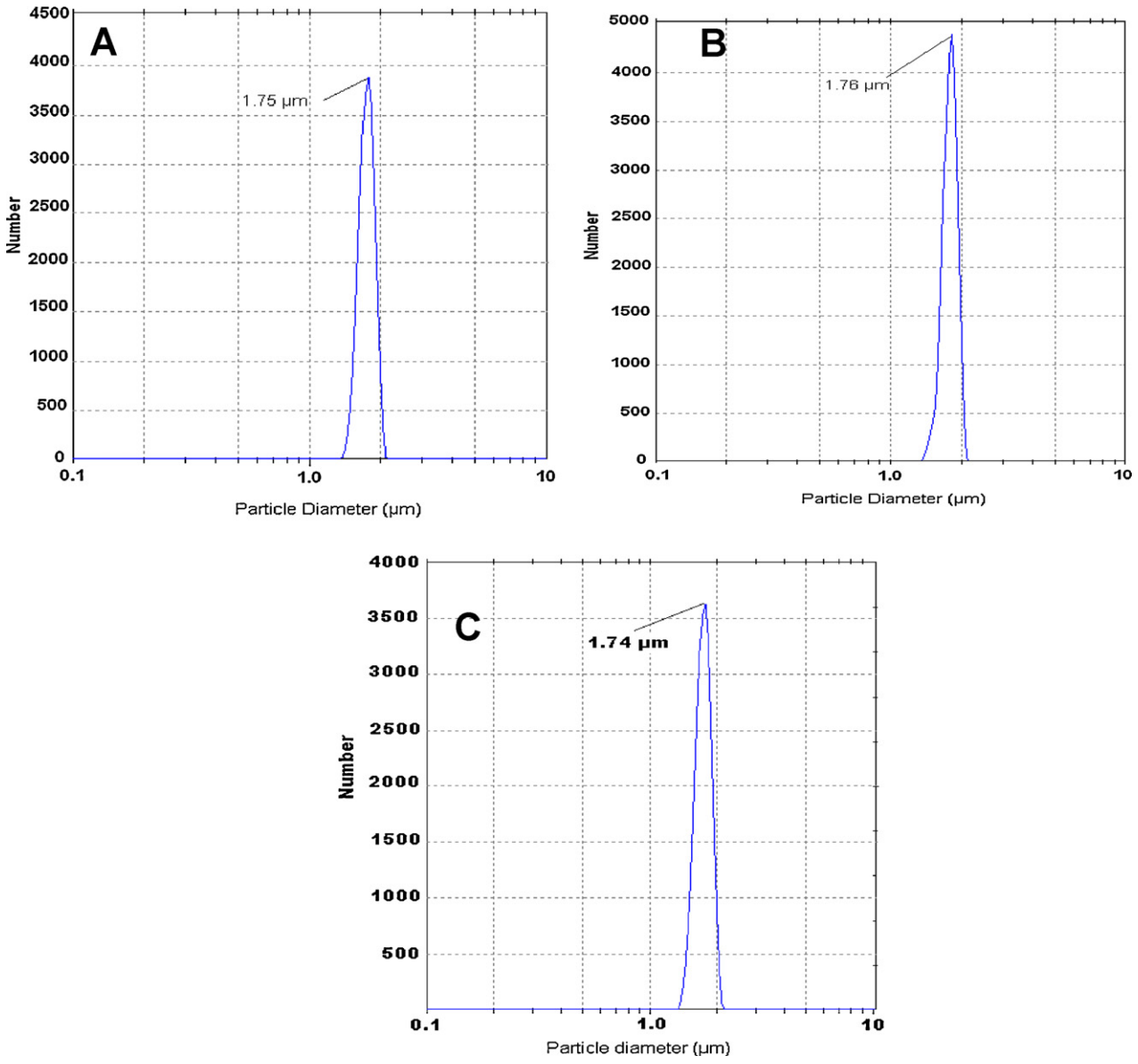

Fig. 2. Particle size distribution analysis for a collection of 4000 EIROSHELL™ particles measured by the Coulter counter technique. (A) EiS-150, (B) EiS-250 and (C) EiS-350. Note the narrow particle size distribution of the EIROSHELL™ particles, the size shown on the graph reflects the mode of the particles, i.e. the most frequently observed particle diameter.

more with the silicon–oxygen atom. Due to a lack of the primary electron beam penetration, the mean free path is very small and the resulting image is seen as very dark. In contrast, scattering of the electron beam around the porous layer of the EiS particles is characterised by a different phenomenon to that in the solid centre core. The electron beam penetrates the porous shell layer due to the existence of the embedded porosity and the electron beam tends to penetrate and interact more within the depth of the shell layers. This produces a revealing image in the porous layer section that seems darker than the solid centre core. The ordered layer-by-layer of the silica shell as revealed by TEM images (Fig. 1) of the EiS particles is due to the systematic approach of preparing the shell particles [14]. The TEM analysis extensively characterises the physical presence of the porous shell layer with well-defined variation of the porous shell layer thickness as shown in Fig. 1Aii–Cii.

The SEM operates at a maximum electron voltage of 20 keV. The back scattered electrons from solid samples are due to the nearly non-penetrating power of the electron beam and the resulting image of the EiS silica particles shows mainly the surface morphology. The volume fraction of the shell layer is paramount for chromatographic application, thus from the TEM image, the porous shell volume fraction of the shell particles $(1-\rho^3)$ of the three EiS particles is 44%, 65% and 80% for the EiS-150, 250 and 350 respectively.

3.1.2. Particle size distribution by electric sensing zone

Fig. 2A–C shows the particle size distribution analysis of the EiS-150, EiS-250 and EiS-350 phases, respectively based on the Coulter counter method. The numbers of particles analysed are 3000–4500 particles and the number average particle diameter (d_{50}) was ~1.75 µm among the three EiS silica particles. However, the difference in the number average particle sizes at 90% and 10% of the total population represents the standard deviation and the ratio of the particle size at this range ($d_{90/10}$) also gives the measure of the uniformity of the particles. The uniformity of the particle is paramount among the EiS particles from the standpoint of the efficiency obtained when they are packed in a given column dimension. Accordingly, all three particles have the same standard

Table 1
Mode (d_{mode}), mean (d_{mean}) and median (d_{50}) diameter of the EiS core–shell particle, $d_{90/10}$ distribution ratio, standard deviation (s) of the mode particle diameter measured from the coulter method for approximately 3500 EiS particles and the percent volume fraction ($1-\rho^3$) of the shell layers of the three EiS particles.

	d_{mode} [μm]	d_{mean} [μm]	d_{50} [μm]	$d_{90/10}$	s (%)	$1-\rho^3$ [%]
EiS-150	1.75	1.79	1.77	1.16	6	44
EiS-250	1.76	1.78	1.77	1.15	5.5	65
EiS-350	1.74	1.79	1.76	1.16	6	79

deviation of ±8% ($d_{90/10}$ = 1.16) for EiS-350, ±8% ($d_{90/10}$ 1.15) for EiS-250 and ±8% ($d_{90/10}$ 1.16) for EiS-150 silica particles. These values are comparable to the two most efficient columns (e.g. the Halo and Kinetex) commercially available core–shell columns [13]. Table 1 shows the three EiS particle mean, median and mode diameters and the distribution ratio together with the volume fraction of the shell layers.

3.1.3. Nitrogen adsorption analysis

Fig. 3A shows the nitrogen sorption isotherms of the three EiS particles as the plot of the volume of gas adsorbed per gram of the adsorbent EiS silica particle at standard temperature and pressure versus relative pressure (P/P_o). Each curve for the EiS silica, shown in Fig. 3A, is composed of the adsorption (lower section of the curve ascending to higher P/P_o indicated by the upward arrow) and desorption (upper section of the curve descending to lower P/P_o indicated by downward arrow) isotherms. The effective surface area (BET method) and pore size distribution (BJH method) can be derived using well defined statistical equations [15,16].

The physio-sorption presented by the three EiS shell particles is representative of type IV with H1 hysteresis loop according to the IUPAC classification [21], characterising the EiS core–shell particle as mesoporous materials.

The specific surface area (SSA) measured by the BET method varies among the three EIROSHELL particles: the EiS-350 had the largest the SSA of 168 m^2/g; the EiS-250 and EiS-150 were 130 m^2/g and 80 m^2/g respectively. The specific pore volume (SPV) of the three materials (0.143 cm^3/g, 0.257 cm^3/g and 0.334 cm^3/g for EiS-150, EiS-250 and EiS-350 respectively) was also determined from the gas sorption analysis method with the results shown in Table 2.

However, the SSA and SPV values given from the BET measurement are not closely related to the true chromatography property of these materials for two well defined reasons:

1. The SSA and SPV are related to a total mass of 1 g of particles composed of a geometrical structure made of non-porous silica, surrounded by a given layer of porous shell of silica. This means the mass of the non-porous silica that virtually has no surface area and contributes significantly to the surface area per gram and present ambiguity in comparing solute retention.
2. The volume fraction of the porous shell silica varies significantly among the three materials (44%, 65% and 80%) due to the size variation of the solid core. This means the constant unit per gram reported from BET sorption analysis is biased among the materials, resulting in unclear results for chromatographic retention properties.

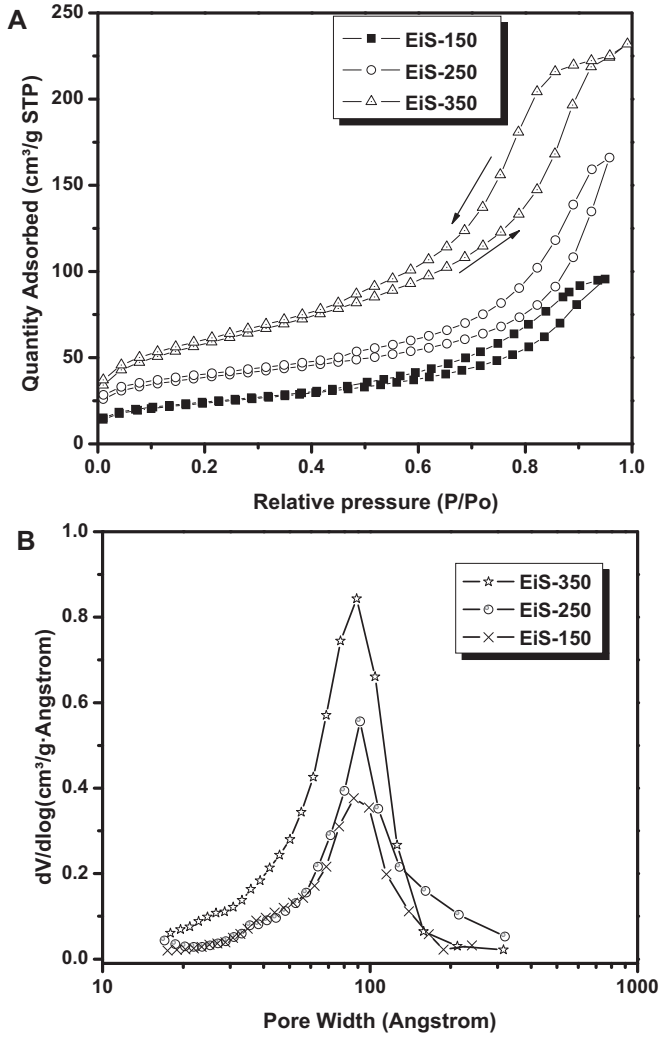

Fig. 3. Gas sorption/porosimetry analysis of the EIROSHELL™: (A) an overlay of the adsorption–desorption isotherm of EiS-150, 250 and 350 silica particles and (B) overlay of the BJH pore size distribution analysis of EiS-150, 250 and 350. Note the typical mesoporous gas sorption isotherm for the EIROSHELL™ particles. Also note the narrow pore size distribution of the EIROSHELL™ particles and the decrease on intensity of the log pore volume per gram scale as the shell thickness decreases from 350 nm to 150 nm.

The corrected data report derived from the BET measurement based on the volume fraction of the porous shell contained in the particles provides the actual representation of the SSA_{shell} and SPV_{shell} as follows [13]:

$$SSA_{shell} = SSA\frac{1-\in_p}{1-\in_{shell,p}}\frac{\in_{shell,p}}{\in_p} \quad (4)$$

where $\in_p$ is the porosity of the shell particle, it is derived from the estimated pore volume V_s, of the packing material inside the column and $\in_{shell,p}$ is the porosity of the shell contained in the shell particles and is given as [13]:

$$\in_p = \frac{V_p}{V_p + (1/p_{sk})} \quad (5)$$

where p_{sk} is the skeletal density of the particles measured by helium pycnometry. It was 2.21 ± 0.0012 g/cm^3 and 1.88 ± 0.0016 g/cm^3 for the unbounded and C_{18} bonded silica.

$$\in_{shell,p} = \frac{\in_p}{(1-\rho^3)} \quad (6)$$

and

$$SPV_{shell} = SPV\frac{1-\in_p}{1-\in_{shell,p}}\frac{\in_{shell,p}}{\in_p} \quad (7)$$

The derived data of the SSA_{shell} and SPV_{shell} from Eqs. (4) and (7) respectively for the three materials (276 m^2/g/0.493 cm^3/g, 251 m^2/g/0.495 cm^3/g and 240 m^2/g/0.479 cm^3/g for the EiS-150, EiS-250 and EiS-350 porous shell silica) are given in Table 2. They are different from the experimental raw values obtained from the BET analysis. The data derived from Eqs. (4) and (7) also provide the

Table 2
Data obtain from nitrogen adsorption analysis; BET surface area (SSA), BJH pore volume (SPV) and pore size (APD).

	EiS-150	EiS-150 C_{18}	EiS-250	EiS-250 C_{18}	EiS-350	EiS-350 C_{18}
SSA [m^2/g]	80	31	130	38	168	44
SPV [cm^3/g]	0.143	0.103	0.257	0.125	0.334	0.133
APD [Å]	91	63	90	64	90	61
Physical properties of the porous shell derived from gas sorption analysis data and ISEC						
SSA_{shell} [m^2/g]	276	80	251	64	240	59
SPV_{shell} [m^2/g]	0.493	0.267	0.495	0.211	0.479	0.177
Total ϵ_t, external ϵ_e and particle ϵ_p porosities measured pycnometry and ISEC						
ϵ_t	0.522	0.448	0.563	0.479	0.588	0.511
ϵ_e	0.396	0.392	0.399	0.394	0.405	0.401
ϵ_p *	0.207 (0.473)	0.092 (0.208)	0.273 (0.420)	0.141 (0.217)	0.305 (0.386)	0.183 (0.230)
V_s [cm^3/g]	0.118	0.054	0.170	0.087	0.199	0.119
ρ_{sk} [g/cm^3]	2.21	1.88	2.21	1.88	2.21	1.88

* The value in parentheses is the porosity of shell layers without taking into account the solid core.

actual SSA and SPV of the shell of the core–silica particles for these columns. The trend seems to increase in SSA and SPV of shell from EiS-350 to EiS-150, although a slight increase in the pore volume of the EiS-250 compared to the EiS-150 and such a result might be partly due to the broader pore size distribution as shown in Fig. 3B.

Narrow pore size distribution is another critical independent parameter augmenting the performance of the column packed with porous silica. Fig. 3B represents the pore size distribution of the three EiS particles from the nitrogen sorption analysis based on the BJH method, showing pore width as a function of log volume of gas adsorbed. As expected, there was a broader pore size distribution for the EiS-250 than the rest of the shell particles. The small mesopore (<40 Å) and large mesopore (>130 Å) are relatively more abundant for the EiS-250, and this is possibly the reason for the relative larger SPV_{shell} of the EiS-250 shell silica particles and very close to that of the EiS-350 type. The EiS-350 particle shows a relatively smaller amount of mesopores above 130 Å, while the mesopore below 40 Å are quite larger. A small change in pore size distribution is due to subtle differences in the preparation of different shell thicknesses [14].

3.1.4. Bonded phase characterization

After functionalisation with octadecyldimethylchlorosilane, subsequent independent and complimentary analysis such as thermogravimetric (TG) and elemental analyses were performed for each EiS particle. The characteristic bonded phases are denoted as EiS-150-C_{18}, EiS-250-C_{18} and EiS-350-C_{18}. Fig. 4 is a TGA graph showing the percentage weight loss of bonded C_{18} as a function of temperature. The significant weight loss ~450–520 °C is an indication of covalent attachments of the silane functional group via the adjacent surface silanol present on the EiS particles. The three EiS-C_{18} particles revealed some variation of weight losses as a result of the difference in the surface area among the EiS-150, 250 and 350 particles. Complimenting the percentage weight loss of carbon using elemental analysis, the values of 5.61%, 7.43% and 8.87% for the EiS-150-C_{18}, 250-C_{18} and 350-C_{18}, respectively, for the percent weight carbon were obtained. This result was also biased by the non-chromatographic important solid-core volume variation among these materials. It is essential that the percent weight carbon should be accounted for the porous shell layer alone and not for the whole particles. The percent weight carbon with respect to the porous shell silica weight inside the column was estimated from Eq. (4) providing a value of 19.33%, 14.32% and 12.71% for the EiS-150, EiS-250 and EiS-350 respectively (Table 3).

The actual carbon surface coverage due to covalent attachment of silane was calculated using the Berendsen de Galan equation [22,23]

$$\alpha = \frac{10^6 p_1}{S_o(100Cn_1 - p_1M_1)} \quad (8)$$

where, p_1, n_1, M_1 are the percentages of carbon contents, the number of carbon atom per anchored group (given as 20 for octade-

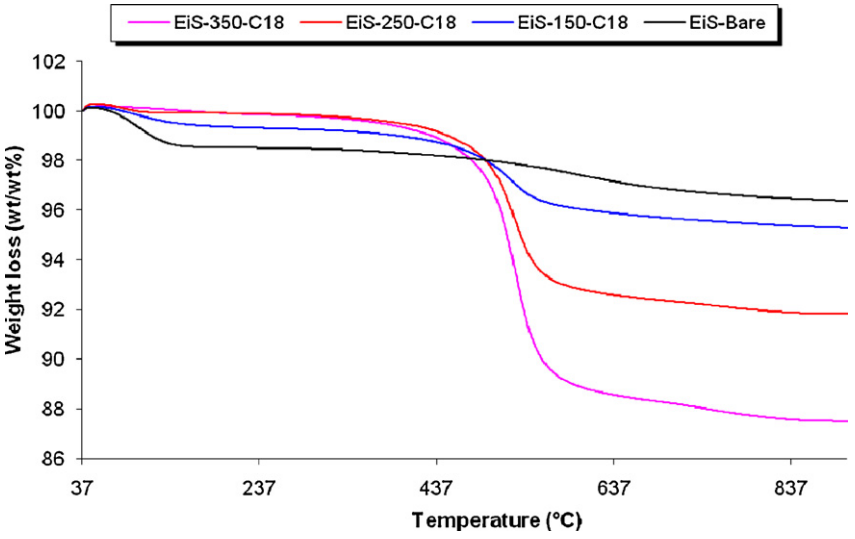

Fig. 4. TGA graph showing % weight loss of C_{18} ligand after functionalisation versus temperature showing line colours that represent the TGA for each shell C_{18} particles (pink line) EiS-350-C_{18} (red line) EiS-250-C_{18}, (blue line) EiS-150-C_{18} (black) unfunctionalised EiS-350. Note the major weight loss at > 500 °C among the three EiS C_{18} phases indicating covalent attachments. (For interpretation of the references to color in this figure legend, the reader is referred to the web version of the article.)

Table 3
Physical characterisation of bonded phase: percent carbon of unmodified (%C_0), percent carbon after C18 derivatisation (%C^1), surface coverage (α), volume of bonded phase (V_{C18}) and phase ratio (β). Values in parentheses are the packing density.

	%C_0	%C^1 [a]	α [μmole/m^2] [b]	Wt. C_{18} [g]/ρ_{bulk} [cm^3/g]	V_{C18} [μL]	β
EiS-150-C_{18}	0.0	19.33	3.89	0.1795 (1.035)	27	0.36
EiS-250-C_{18}	0.0	14.32	2.94	0.1695 (0.978)	21	0.26
EiS-350-C_{18}	0.0	12.71	2.64	0.1589 (0.917)	16	0.18

Wt (g). of columns measured prior to vacuum drying: EiS-150-C_{18} = 0.3154, EiS-250-C_{18} = 0.3188, and EiS-350-C_{18} = 0.3217.
[a] % wt carbon with respect to porous shell weight inside the column.
[b] Surface coverage of porous shell silica.

cyldimethylchlorosilane) and the molecular weight of anchored group present after the primary bonding. S_o, and C are the surface area of the silica and atomic weight of carbon (given as 12 g/mol), respectively. The carbon surface coverage of 3.89, 2.92 2.64 μmole/m^2 on the porous shell of the core–shell particles were obtained for the EiS-150-C_{18}, EiS-250-C_{18} and EiS-350-C_{18}, respectively (Table 3).

3.1.5. Column porosity measurement

The three EiS C_{18} particles were packed in 2.1 I.D. × 50 mm columns using the slurry packing technique [18]. The total porosity was determined based on the packing density of each stationary phase inside the column. The masses of packing materials were determined by first weighing the empty column tubes then, after the column packing the resulted packed columns were vacuum dried to ensure complete removal of the packing solvent. The weight masses of the columns containing the dried packing material were measured and the obtained masses of the empty column tube were subtracted from these to give the masses of the EiS-C_{18} packing materials in the columns. The masses of 0.1795, 0.1695 and 0.1589 g obtained correspond to the packing densities of 1.037, 0.978 and 0.918 g/cm^3 for the EiS-150-C_{18}, EiS-250-C_{18} and EiS-350-C_{18} in the 2.1 I.D. × 50 mm column.

The volume of the empty column tube (V_{col}) is equivalent to 0.1732 cm^3. The total porosity is calculated as follows:

$$\in_t = 1 - \frac{\rho_{bulk}}{\rho_{sk}} \quad (9)$$

where ρ_{bulk} is the bulk density of the EiS silica packing material. The total porosity value for the EiS-150-C_{18}, EiS-250-C_{18} and EiS-350-C_{18} was 0.448, 0.479 and 0.511, respectively. The increase in porosity from EiS of 150 to 350 is due to the reduction in volume of the solid core in that order. The total porosities of the unfunctionalised EiS columns were also measured as shown in Table 2 and the differences in the values obtained are due to the presence of the C_{18} chains.

The external porosities $\in_e$ of the three EiS-C_{18} columns were measured by inversed size exclusion chromatography (ISEC) [24]. A similar method employed in this study is described in Ref. [2], typically we employed 12 polystyrene standard (MW = 472–2,180,000). Fig. 5 shows the plots of the elution volume of the 12 polystyrene standards from the different C_{18} columns versus the cube root of the molecular weight (MW$^{1/3}$). Extrapolation of the exclusion branch of the ISEC plot to MW$^{1/3}$ = 0 gives the column external volume $V_{ext.}$ of the column, thus the external porosity $\in_e$ is derived with following relationship:

$$\in_e = \frac{V_{ext.}}{V_{col}} \quad (10)$$

Table 2 shows the $\in_e$ of the EiS particle and the values were never above 0.4 for both unfunctionalised and C_{18} modified packed columns revealing the intrinsic properties related to the surface smoothness.

The shell porosity for the unmodified ($\in_{p,shell,0}$) and modified ($\in_{p,shell}$) EiS particles are given in Table 2, a characteristic of the variation of the solid core silica volume. The presence of the C_{18} bonded material imparted a significant reduction of the particle porosity, for example, the $\in_{p,shell,0}$ of the EiS-150 packed column decreased from 0.207 to $\in_{p,shell}$ = 0.092 and similar trend is found for the other EiS shell particles studies (see Table 2). The volume of the bonded stationary phase V_{C18}, was estimated from the porosity reduction due to the presence of the bonded C_{18} as follows [8]:

$$V_{C18} = (1 - \in_e)(\in_{p,shell,0} - \in_{p,shell})V_{col} \quad (11)$$

From the value of the V_{C18}, the phase ratio β, is deduced (i.e. the volume fraction of the packed column occupied by the C_{18} phase to the mobile phase eluent).

The EiS-150-C_{18} column exhibited the largest % phase ratio of 36 compared with 18 for the EiS-350-C_{18} column. The different values of the phase ratios are correlated to the different values of the porous shell surface coverage achieved as shown in Table 3.

3.2. Kinetic performance of the EiS-150-C_{18}, EiS-250-C_{18} and EiS-350-C_{18}

The reduced HETP values obtained with naphtho[2,3-a]pyrene with different mobile phase conditions on the three C_{18} EiS columns provided a similar retention factors k'. The diffusion coefficient estimated by Eq. (1) becomes 6.21 × 10^{-6}, 8.42 × 10^{-6} and 1.11 × 10^{-5} cm^2/s for the EiS-150-C_{18}, EiS-250-C_{18} and EiS-350-C_{18} columns, respectively.

The extra-column volume variance ($\mu'_{2,ex}$) of the Agilent 1200 RRLC measured from a half peak width of naphtho[2,3-a]pyrene with mobile phases was given. Fig. 6 shows the plot of the flow

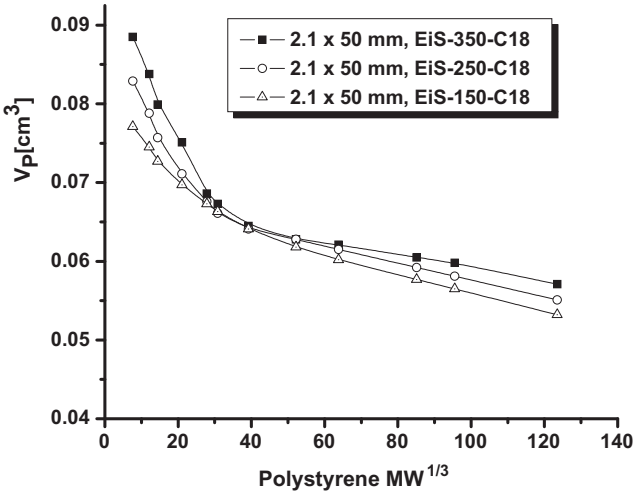

Fig. 5. Overlay of the inverse size exclusion chromatography (ISEC) on columns (2.1 I.D. × 50 mm) packed with three EIROSHELL™ C_{18} particles (EiS-150, EiS-250 and EiS-350) by injecting 0.3 μL successively of 12 different polystyrene standards (MW = 472; 1920; 3250; 10,250; 24,000; 32,500; 67,500; 160,000; 295,000; 705,000; 1,000,000; and 2,180,000) at flow rate of 0.35 mL/min at 25 °C. Note the similar exclusion branch indicating identical internal pore size of the three EiS-C_{18} particles.

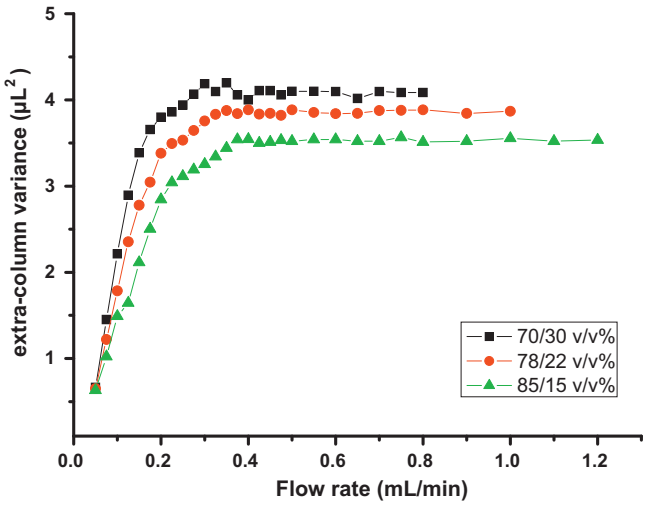

Fig. 6. Comparison of the plot of the extra-column variance of naphtho[2,3-a]pyrene as a function of the flow rate for different compositions of acetonitrile and water mobile phase that was employed for the HETP data analysis (full square) 70/30 (v/v%) (full circle) 78/22 (v/v%) and (full triangle) 85/15 (v/v%). Note the effect of increasing the acetonitrile composition to smaller extra-column contribution.

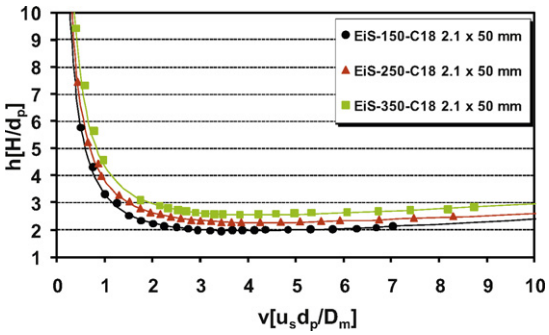

Fig. 7. Comparison between the plots of the reduced HETP, h, versus the reduced linear velocity, ν, for naphtho[2,3-a]pyrene on the three EiS-C_{18} column (full square) EiS-350-C_{18} using 85/15 (v/v%) of acetonitrile/water mobile phase (full triangle) EiS-250-C_{18} using 78/22 (v/v%) of acetonitrile/water mobile phase and (full circle) EiS-150-C_{18} using 70/30 (v/v%) of acetonitrile/water mobile phase.

rate at 0.05–1.2 mL/min *vs.* the extra-column variance (in volume) of the three mobile phase conditions. The $\mu'_{2,ex}$ was estimated for each flow rate using Eq. (3). Between 0.2 and 1.2 mL/min, the extra-column variance did not exceed: 4.0 μL^2 (for the 70/30 (v/v%) of acetonitrile/water), 3.8 μL^2 (for the 78/22 (v/v%) of acetonitrile/water) and 3.4 μL^2 (for the 85/15 (v/v%) of acetonitrile/water). The reason why the extra-column variance of the 85/15 (v/v%) acetonitrile water is the smallest among the three eluent used is due to its low viscosity, leading to a large molecular diffusion coefficient of the test solutes. This ultimately results in a decrease in band broadening inside the tubing, thus leading to a narrower peak band width. This is much smaller than the extra-column volume measured with columns connected, 13 μL^2, 17 $\mu L^2$and 19 μL^2 for the EiS-150, 250 and 350-C_{18} (at the maximum flow rates) and correspond to an extra-column contribution that accounts for nearly, 30%, 23% and 18% loss of efficiency, respectively. Notice that Eq. (3) employed for the correction of the contribution to extra-column volume is a poorer estimation due to the fact that the peak shape eluting from the zero-volume connector is not perfect Gaussian. The net result is that the extra-column volume of the system could be underestimated and the actual extra-column volume could be much higher than value reported here. A true approximate estimate of the band broadening contribution can be achieved by employing the moment analysis methods as suggested by Gruska [25] or the Foley–Dorsey equation [26].

The HETP data for each column at different mobile phase compositions were obtained using Eq. (2). Fig. 7 shows a plot of the reduced HETP *vs.* the reduced linear velocity of the three EiS-C_{18} columns. The retention factors were 9.61, 10.34 and 10.37 for the EiS-150, 250 and 350-C_{18} columns, respectively, achieved by using different eluent mobile phases for each column. The Henry constant (K_{shell}) for the distribution coefficient of the solute between the eluent and the porous shell of the core–shell particles at the same retention factor was corrected for the diffusion coefficient (D_m) of the solute given according to the following equation [13].

$$K_{shell} = \frac{\in_t k}{(1 - \in_e)(1 - \rho^3)(1 - \in_{shell,p})} \quad (12)$$

The $K_{shell,\text{EiS-150-C18}} = 20.31$, $K_{shell,\text{EiS-250-C18}} = 16.08$ and $K_{shell,\text{EiS-350-C18}} = 11.42$ and the minimum reduced HETP ($h_{\min}$) for the three EiS columns was 1.9, 2.2 and 2.5, respectively. The coefficients of the HETP, the molecular diffusion coefficient of naphtho[2,3-a]pyrene based on the three mobile phase compositions and the ratio of the effective diffusivity to bulk molecular diffusion coefficient (Ω) are given in Table 4.

The reduced B-term contribution to $h_{\min}$ was 0.45, 0.66 and 0.79 for the EiS-150 to 350-C_{18} columns, respectively. This is due to: (a) the different thickness of the shell particles and ultimately the larger solid core particle would avert the diffusion of the solute across a significant part of the column and a smaller B-term is the result. The smaller solid core diameter with a larger shell thickness provides the propensities of the solute to diffuse across large column areas, (b) the shell porosity ($\in_{p,shell}$) is govern by the shell thickness, the smaller this value the less time solute tends to spend inside the column and spreading of the band becomes smaller and (c) the distribution coefficient of the solute between the eluent and the adsorbent is largest for the EiS-350-C_{18} column having the largest shell thickness and is smallest for the EiS-150-C_{18} column with the smallest shell thickness. The B-terms for the three EiS-C_{18} columns were confirmed using the peak parking experiment [27].

The A-terms obtained from the fit of experimental HETP plots were found to vary with the shell thickness. The smallest A-term was observed for the EiS-150-C_{18} (1.44) and the largest A-term for the EiS-350-C_{18} (1.70) under the same retention factor. This rather suggests that the intrinsic variation in the shell thickness of the three EiS-C_{18} particles does affect the A-term.

This trans-column velocity bias causes a strong local concentration gradient of solutes, hence distorting the solute band that elutes from the column. This is the main cause of the eddy diffusion (A-term) particularly from columns that are packed with

Table 4
Best fit for the HETP parameter for naphtho[2,3-a]pyrene (A, B and C) on the three EiS-C_{18} column with the given optimum reduced velocity (ν_{opt}), molecular diffusion coefficient (D_m) and ratio of effective diffusivity to bulk molecular diffusion coefficient of naphthalene (Ω), estimated from PP method.

	A	*B*	*C*	*k'*	$h_{\min}$	ν_{opt}	D_m [cm²/s]	$\Omega_{\text{Na-p}}$
EiS-150-C_{18} 2.1 × 50 mm	1.44	1.55	0.031 (0.027)	9.61	1.9	3.44	6.21×10^{-6}	0.61
EiS-250-C_{18} 2.1 × 50 mm	1.54	2.29	0.053 (0.042)	10.34	2.2	3.44	8.42×10^{-6}	0.72
EiS-350-C_{18} 2.1 × 50 mm	1.70	3.06	0.073(0.056)	10.37	2.5	3.83	1.11×10^{-5}	0.83

In parentheses are given the theoretical values of the trans-particle mass transfer term according to Eq. (13).

particles of narrow particles size distribution, peculiar to the three EiS-C_{18} particles currently studied. The recent work by Gritti and Guiochon [28] has demonstrated that an increase in retention tends to relax the local concentration gradient from a radially heterogeneous packed bed. This phenomenon of retention allows the solutes to have sufficient time to reach a concentration equilibrium state in the entire stream path of the packed bed and produces a well defined distribution of eluted solute bands. Consequently, the A-term caused by the trans-column velocity biases is significantly alleviated by an increase in retention.

The radial trans-column velocity biases inside the three EiS-C_{18} packed beds are expected to be of the same order since their particle diameter is the same. In addition the ISEC measurement confirmed that the particles were smooth surfaced material, thus the packed bed for the three EiS-C_{18} particles could have the same order of heterogeneity. The similar retentivity of the three EiS-C_{18} columns employed would essentially mean the same A-term (if trans-column velocity biases governs the A-term). The three EiS-C_{18} particles are equally well packed under the same conditions. In addition, the particles packed on a narrow bore column indeed play a vital role in the overall packing quality and efficiency [8]. The A-term for the EiS-150-C_{18} is 1.44 and that of the EiS-350-C_{18} is 1.70; this clearly illustrates that the presence of the solid core has a vital role in governing the A-terms despite at the same retentivity. In short, the variation in the structural geometry of the three EiS core-shell particles governs the solute transport from diffusive point-to-point within the stagnant mobile phase inside the pores.

Most importantly, dispersion tends to alleviate a radial concentration gradient; we assume the EiS-150-C_{18} has the largest radial dispersion coefficient of solutes due to its largest volume of non-porous solid core. A meaningful conclusion to the A-terms from these three EiS-core–shell particle columns is that at the same retention coefficient, the EiS-150-C_{18} has the largest dispersion coefficient among the rest of the EiS-columns; this would effectively minimize the transcolumn velocity. The increased solid core volume tends to be more important in relaxing the flow velocity inequality from one point of a particle distance to another. Nevertheless, further measurements are essential to obtain experimental data to explain this unusual scenario.

The intraparticle diffusivity is an important parameter that influences the C-term [2] and more importantly the diffusive path length (shell thickness). The C-term did not vary significantly among the three EiS-C_{18} columns; however it was smallest for the EiS-150-C_{18} column, 2.3-fold smaller than the EiS-350-C_{18} column and only 1.6-fold larger than the EiS-250-C_{18}. A theoretical consideration of the mass transfer resistance term would justify the C-terms of the three shell columns obtained from the Knox model. Due to the smooth particle surface of the material studied, the external film mass transfer is negligible and the trans-particle mass transfer is more important and can be expressed as follows [10]:

$$C_p = \frac{1}{30\Omega}\frac{\in_e}{1-\in_e}\left[\frac{k_1}{1+k_1}\right]^2\frac{1+2\rho+3\rho^2-\rho^3-5\rho^4}{(1+\rho+\rho^2)^2}\nu \qquad (13)$$

where k_1 is the zone retention factor given by [11]:

$$k_1 = \frac{1-\in_e}{\in_e}\left[\in_{shell,p}+(1-\in_{shell,p})K_{shell}\right](1-\rho^3) \qquad (14)$$

The theoretical trans-particle mass transfer terms (C_p) for the EiS-150-C_{18}, EiS-250-C_{18} and EiS-350-C_{18} columns were 13%, 19% and 23% respectively smaller than the overall C-term fitted in the Knox model (Table 4). Thus, we can conclude that:

1. The porous shell material studied tends to have a slight increase in the surface roughness with increasing shell thickness as predicted from the ISEC measurement where it increases from 0.392 to 0.405 (Table 2).
2. The overall C-terms of the three EiS-C_{18} columns are governed mainly by the trans-particle mass transfer resistance.

The C-term constant for the three EiS-C_{18} columns is not strongly affected by the variation in the shell thickness for small molecules such as naphtho[2,3-a]pyrene.

3.3. Separation of a test mixture on the EiS-350-C_{18}, EiS-250-C_{18} and EiS-150-C_{18} columns

Fig. 8 shows the chromatogram for the five text compounds eluted from the three EiS-C_{18} columns. The extra-column variance contributions on these columns are expected to vary significantly, taking into account the different column hold-up volumes. The Agilent 1200 RRLC has an extra-column volume of 10.5 μL (first moment in volume) and 4.0 μL^2 (second central moment in volume). To compare the impact of extra-column contributions, the total variances of the non-retained solute uracil are 76.1 (EiS-150-C_{18}), 83.6 (EiS-250-C_{18}) and 89.8 (EiS-350-C_{18}) μL for the first moment and 5.1 (EiS-150-C_{18}), 5.7 (EiS-250-C_{18}) and 6.3 (EiS-350-C_{18}) μL^2 for the second central moment. As expected, the extra-column band broadening contributions account for ~80%, 70% and 63% of the total peak variance for the non-retained solute uracil on the EiS-150-C_{18}, EiS-250-C_{18} and EiS-350-C_{18}, respectively. The retained solute naphthalene (the last eluting peak in Fig. 8) was 146, 216 and 320 μL, respectively for the first moment and 16.1, 30.5 and 58.1 μL^2, respectively for the second central moment. This ultimately produces an extra-column band broadening contribution of 25, 13 and 7% of the total peak variance of naphthalene for the EiS-150-C_{18}, EiS-250-C_{18} and EiS-350-C_{18}, respectively. The efficiency measured on the Agilent 1200 RRLC system is 75%, 87% and 93% of the maximum efficiency of naphthalene. For uracil, this values decreases significantly to 37%, typically for non-retained compounds in narrow bore columns [8]. Accordingly, the efficiency (N/m) of the last eluting peak naphthalene was 306,500 *vs.* 245,200 for the EiS-150-C_{18}, 247,700 *vs.* 219,220 for the EiS-250-C_{18} and 208,920 *vs.* 195,640 for the EiS-350-C_{18} for the corrected *vs.* un-corrected extra-column variance contribution, respectively. Table 5 shows the chromatographic data including the efficiency (N/m) and the retention coefficient of the five test solutes separated on the three EiS-C_{18} (2.1 × 50 mm) columns. The early eluted compounds such as uracil and acetophenone ($k' < 1$) on the EiS-150-C_{18} column have smaller efficiency compared to the EiS-250-C_{18} and EiS-350-C_{18} columns. This observation is ascribed to a larger hold up volume (10–15%) of the thicker porous shell compared to the EiS-150-C_{18} column. In addition, as the peak widths of solutes are much narrower for the EiS-150-C_{18} column, they are more sensitive to extra-column contribution particularly for the almost non-retained solutes. The less retained solutes are also affected significantly by eddy diffusion as the local radial concentration gradient is not relaxed via retention and trans-column velocity biases become severe [28].

The true performance of highly efficient columns attributed to a very thin porous shell is significantly deteriorated by the system extra-column contribution to band broadening. The thinner the porous shell layer the smaller the column hold-up volume and this makes a solute eluting from thin porous shell layer columns more sensitive to system extra-column volume particularly for the early eluting compounds ($k' = <1$). Notwithstanding, it is very important to take into account and subtract the contribution to band broadening caused by the instrument on the columns packed with shell particles, with thin shell layers in narrow bores and short lengths of columns, e.g. EiS-150-C_{18}, to allows a true estimation of efficiency.

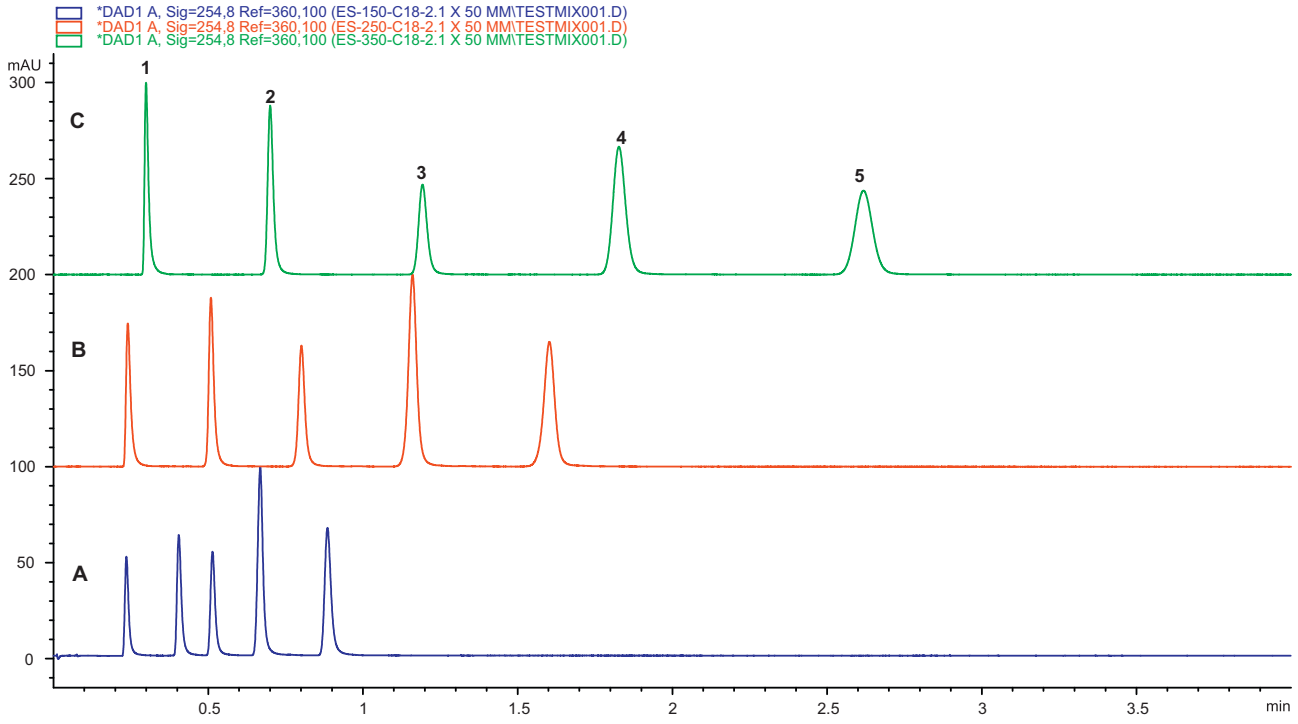

Fig. 8. Separation of five test solutes on three EiS-C_{18} packed on 2.1 × 50 mm columns (A) EiS-150-C_{18}, (B) EiS-250-C_{18} and (C) EiS-350-C_{18}. Eluent: 50/50 (v/v%) acetonitrile/water. Flow rate: 0.4 mL/min. T = 25 °C. Detection: UV = 254 nm. Sample: (1) uracil, (2) acetophenone, (3) benzene, (4) toluene, and (5) naphthalene.

Table 5
Chromatographic data of efficiency (N/m) and retention coefficient (k') for five compounds separated on the three EiS-C_{18} column.

N/m and k':	Uracil	Acetophenone	Benzene	Toluene	Naphthalene
EiS-150-C_{18}	41,894/0.0	105,411/0.7	165,562/1.18	199,564/1.83	245,220/2.75
EiS-250-C_{18}	51,562/0.0	128,225/1.12	163,520/2.33	188,520/3.83	219,220/5.66
EiS-350-C_{18}	59,562/0.0	144,700/1.34	162,580/2.99	187,840/5.11	195,640/7.76

4. Conclusion

This study has evaluated some important structural parameters of core–shell (EIROSHELL™) particles with different porous layer thickness on a solid-core. The structural differences obtained from the SEM, TEM, BET and BJH pore size analysis revealed that the porous layer thickness plays a major role in governing the porosity of the EIROSHELL™ particles. ISEC data indeed confirm that the EIROSHELL™ consists of smooth external surfaces. The HETP study evaluated under the retention factor for the three EiS-C_{18} columns, logically clarifies their difference in the A-term among the three columns. Although no sufficient experimental data at this stage prove that solid-core volume plays a governing role in the A-term. The reduced plate height of $h_{min} \sim 1.9$ achieved for the EiS-150-C_{18} is the most efficient sub-2 μm particle narrow bore packed column reported. The reason for this superior performance is correlated to the shell thickness.

The extra-column contribution to band broadening plays an important role in the efficiency of the solute band eluting from the columns causing a major loss in efficiency on column with less retentivity, e.g. the EiS-150-C_{18} column. The extra-column contribution that contributes to nearly 30% and 70% loss in efficiency for well retained and non-retained solutes, respectively for the EiS-150-C_{18}, only contributes about 30% relatively less for the EiS-350-C_{18} to that of the EiS-150-C_{18}. The estimate of the extra-column contribution reported in this paper is smaller than the actual value of estimate if the moment analysis or the Foley–Dorsey [26] equation is employed.

This works provides clear evidence to highlight the need for both LC system and column manufacturers to work together to collectively design suitable LC systems targeted to deliver the optimum performance of analytical columns that are emerging for modern liquid chromatographic separation.

Acknowledgments

The authors would like to thank Enterprise Ireland (for Grant EI CFTD/06/IT306) under the Commercialisation Fund for Technology Development and also Science Foundation Ireland (Grant Number 08/SRC/B1412) for research funding of the Irish Separation Science Cluster (ISSC) under the Strategic Research Cluster programme.

References

[1] J.J. DeStefano, T.J. Langlois, J.J. Kirkland, J. Chromatogr. Sci. 46 (2008) 254.
[2] F. Gritti, A. Cavazzini, N. Marchetti, G. Guiochon, J. Chromatogr. A 1157 (2007) 289.
[3] S. Fekete, J. Fekete, K. Ganzler, J. Pharm. Biomed. Anal. 49 (2009) 64.
[4] J.M. Cunliffe, T.D. Maloney, J. Sep. Sci. 30 (2007) 3104.
[5] E. Oláh, S. Fekete, J. Fekete, K. Ganzler, J. Chromatogr. A 1217 (2010) 3642.
[6] F. Gritti, G. Guiochon, J. Chromatogr. A 1217 (2010) 1604.
[7] F. Gritti, I. Leonardis, S. David, P. Stevenson, A. Shalliker, G. Georges, J. Chromatogr. A 1217 (2010) 1589.
[8] F. Gritti, G. Guiochon, J. Chromatogr. A 1217 (2010) 5069.
[9] K. Horváth, F. Gritti, J.N. Fairchild, G. Guiochon, J. Chromatogr. A 1217 (2010) 6373.
[10] K. Miyabe, G. Guiochon, J. Chromatogr. A 1217 (2010) 1713.
[11] F. Gritti, C.A. Sanchez, T. Farkas, G. Guiochon, J. Chromatogr. A 1217 (2010) 3000.

[12] K. Kaczmarski, G. Guiochon, Anal. Chem. 79 (2007) 4648.
[13] F. Gritti, I. Leonardis, J. Abia, G. Guiochon, J. Chromatogr. A 1217 (2010) 3819.
[14] J.O. Omamogho, J.D. Glennon, A process for preparing silica microparticles, Patent Pub. No.: WO/2010/061367.
[15] S. Brunauer, P.H. Emmett, E. Teller, J. Am. Chem. Soc. 60 (1938) 309.
[16] E.P. Barrett, L.G. Joyner, P.P. Halenda, J. Am. Chem. Soc. 73 (1951) 373.
[17] C.d.F.v. Hohenesche, V. Ehwald, K.K. Unger, J. Chromatogr. A 1025 (2004) 177.
[18] J.J. Kirkland, J.J. DeStefano, J. Chromatogr. A 1126 (2006) 50.
[19] C.R. Wilke, P. Chang, Am. Inst. Chem. Eng. J. 1 (1955) 264.
[20] S.R.S. Sastri, M. Swati, K.K. Rao, Can. J. Chem. Eng. 74 (1996) 170.
[21] K.S.W. Sing, D.H. Everett, R.A.W. Haul, L. Moscou, R.A. Pierotti, J. Rouquerol, T. Siemieniewska, Pure Appl. Chem. 57 (1985) 603.
[22] G.E. Berendsen, L. de Galan, J. Liq. Chromatogr. Relat. Technol. 1 (1978) 561.
[23] G.E. Berendsen, K.A. Pikaart, L. de Galan, J. Liq. Chromatogr. Relat. Technol 3 (1980) 1437.
[24] M. Al-Bokari, D. Cherrak, G. Guiochon, J. Chromatogr. A 975 (2002) 275.
[25] E. Grushka, Anal. Chem. 44 (1972) 1733.
[26] J.P. Foley, J.G. Dorsey, Anal. Chem. 55 (1983) 730.
[27] F. Gritti, G. Guiochon, Chem. Eng. Sci. 61 (2006) 7636.
[28] F. Gritti, G. Guiochon, AIChE J. 56 (2010) 1495.